PLANAR EFFECTS IN MIM CAPACITORS

F. Giannini, G. Bartolucci, E. Limiti

Dipartimento di Elettronica, II Università di Roma
Via O. Raimondo, 8 - 00173 Roma, Italy

Abstract

Planar effects in MIM capacitors have been investigated, and a novel equivalent circuit has been derived, which allows to take into account any port misalignment.

Keywords: MIM, Planar Effects, Equivalent Circuit

1. Introduction

The MIM capacitor is one of the most widely used component in microwave and millimeter wave integrated circuits (fig. 1). For this reason in the last years many models have been presented, also including some physical fundamental effects. In particular, two different approaches are suggested in the literature: the distributed element approach [1], and the physical lumped modelling approach [2]. On the other hand, many foundries have developed their own models, normally based on curve-fitting measuring procedures. All the so obtained equivalent circuits do not take into account the intrinsic planar behaviour of the structure. In order to overcome this limit, a novel approach is proposed in this paper. The MIM capacitor structure is represented as a cascade of three blocks: the airbridge, the series connected planar capacitor, cascaded to a two-port network, representing the bottom patch. Comparison among experimental data and simulated results, obtained using the proposed model, demonstrate the effectiveness of our approach.

2. Theoretical model and equivalent circuit

As mentioned earlier, the MIM capacitor in fig. 1 is divided into three parts and the equivalent circuit of the entire structure is shown in fig. 2. The first block, the airbridge section, is modelled as a microstrip transmission line, with an equivalent dielectric constant of a bilayered dielectric substrate [3]. A simple expression of the equivalent dielectric constant is given by:

$$(1) \quad \varepsilon_{eq} = \frac{(h+d)\varepsilon_a \varepsilon_s}{\varepsilon_a h + \varepsilon_s d}$$

where ε_a and ε_s are the dielectric constants of the layered substrates of thickness **d** (air) and **h** respectively. The main capacitor is modelled as a parallel-plate one, with geometrical dimensions and dielectric constant replaced by the effective ones [4]:

$$C_{mim} = \varepsilon_o \varepsilon_{r_{eff}} \frac{l_{eff} b_{eff}}{d} \quad (2)$$

A series connected inductor has been added, in order to take into account the residual planar effect of the upper plate. In many practical cases, this inductor assumes negligible values, and, however, can be computed with the same procedure applied for the analysis of the third part.

The last one represents the bottom patch and can be modelled by a rectangular resonator enclosed by lateral magnetic walls and geometrical dimensions and dielectric permittivity replaced by the corresponding effective ones, like in [5]. The electromagnetic field in this resonator is expanded in series of resonant modes, obtaining, for the **Z** parameters of the two-port the following expressions:

$$Z_{11} = \frac{1}{b_{eff} l_{eff}} \frac{1}{j\omega\mu\varepsilon_{oo}} + \frac{j\omega\mu h}{b_{eff} l_{eff}} \sum_m \sum_n \frac{\delta_m \delta_n f_{1n}^2}{(\omega_{mn}^2 - \omega^2)\mu\varepsilon_{mn}} \quad (3)$$

$$Z_{12} = Z_{21} = \frac{1}{b_{eff} l_{eff}} \frac{1}{j\omega\mu\varepsilon_{oo}} + \frac{j\omega\mu h}{b_{eff} l_{eff}} \sum_m \sum_n \frac{(-1)^n \delta_m \delta_n f_{1n} f_{2n}}{(\omega_{mn}^2 - \omega^2)\mu\varepsilon_{mn}} \quad (4)$$

$$Z_{22} = \frac{1}{b_{eff} l_{eff}} \frac{1}{j\omega\mu\varepsilon_{oo}} + \frac{j\omega\mu h}{b_{eff} l_{eff}} \sum_m \sum_n \frac{\delta_m \delta_n f_{2n}^2}{(\omega_{mn}^2 - \omega^2)\mu\varepsilon_{mn}} \quad (5)$$

where

- **m,n** cannot be contemporary equal to zero;
- b_{eff}, l_{eff} are the effective dimensions corresponding to **b** and **l** respectively;
- ε_{mn}, ω_{mn} are the effective permittivity and the angular resonant frequency of the **(m,n)th** mode;
- δ_m is the Neumann factor given by:

$$\delta_m = \begin{cases} 1 & \text{if} \quad m = 0 \\ 2 & \text{if} \quad m \neq 0 \end{cases}$$

and

$$f_{in} = \begin{cases} \cos\dfrac{n\pi p_i}{b_{eff}} \dfrac{\sin\dfrac{n\pi w_{i,eff}}{2b_{eff}}}{\dfrac{n\pi w_{i,eff}}{2b_{eff}}} & \text{if} \quad n \neq 0 \\ 1 & \text{if} \quad n = 0 \end{cases} \qquad i = 1,2$$

These expressions, under the assumption that the operating frequency is much smaller than the modal resonant frequencies, can be reduced to:

$$(6)\quad Z_{11} = \frac{1}{j\omega C_{par}} + j\omega L_1$$

$$(7)\quad Z_{12} = Z_{21} = \frac{1}{j\omega C_{par}} + j\omega M$$

$$(8)\quad Z_{22} = \frac{1}{j\omega C_{par}} + j\omega L_2$$

where $L_{1,2}$ and **M** are practically frequency independent and are evaluated at midband.

From this, the equivalent circuit shown in fig. 2 results.

3. Results and discussion

The validity of the proposed model has been tested comparing the simulated results with experimental data (Courtesy of GMMTL) for an overlay capacitor with h=200μm,d=0.13μm,b=300μm,l=300μm,ε_s=12.9,ε_a=7 and w=144μm, with the results shown in fig. 3.

In order to demonstrate the effectiveness of the planar approach, the port positioning has been changed in two different ways, for a MIM capacitor with h=100μ, d=0.13μm, b=250μm, l=70μm, ε_s=12.9, ε_a=7 and w=20μm.

a. According to fig. 4a, antisymmetrical port positioning has been analyzed, resulting in quite different behaviour of the scattering parameters, as shown in fig. 4b; more in detail, these differences are significant for the phase (fig. 4c), where the capacitive behaviour changes to an inductive one, for particular port positioning. These differences are ascribed to the bottom patch, whose parameter values are plotted in fig. 4d as a function of the port position.

b. According to fig. 5a, the ports are shifted of the same quantity in the same direction with respect to the central plane of symmetry and the behaviour of the equivalent circuit parameters of the bottom patch is plotted in fig. 5b.

As suggested by the geometry of the structure, the curves plotted in figs. 4d and 5b, representing the inductive parasitics, are symmetrical with respect to central positioning of the ports. Moreover, while $L_{1,2}$ (dashed curves) assumes the same values for equal displacement, the coupling coefficient **M** (continuous curves) is always negative for the first case, while it changes sign in the second one, exhibiting a maximum coupling between the two ports.

A comparison, with the same capacitor, has been reported in fig. 6 for three different port positions: centered on the 250μm side, centered on the 70μm side, and antisymmetrically 100μm shifted on the 250μm side; the second case and the third one exhibit similar behaviour, so stressing the necessity of a planar analysis of the overlay capacitors.

4. Conclusions

Planar effects in MIM capacitors have been investigated, leading to a novel equivalent circuit for this structure, which effectively takes into account the changes in the overall characterization of this component, due to the port positioning.

References

[1] - J.P. Mondal, "An Experimental Verification of a Simple Distributed Model of MIM Capacitors for MMic Applications", *IEEE Trans. on MTT*, Vol. MTT 35, April 1987, pp. 403-408.

[2] - H. Do Ky et al., "Physical Lumped Modelling of Thin Film MIM Capacitors", *Proceedings of the 20th European Microwave Conference*, Budapest, September 1990, pp. 1270-1275.

[3] - W. Lam et al., "Experimental Modelling for Millimeter Wave Monolithic Integrated Circuit Components", *Proceedings of MTT Symposyum*, New York, May 1988, pp. 477-480.

[4] - I. Wolff et al., "Rectangular and Circular Microstrip Disk Capacitors and Resonators", *IEEE Trans. on MTT*, Vol. MTT 22, October 1974, pp. 857-864.

[5] - G. D'Inzeo et al., "Method of Analysis and Filtering Properties of Microwave Planar Networks", *IEEE Trans. on MTT*, Vol. MTT 26, July 1978, pp. 462-471.

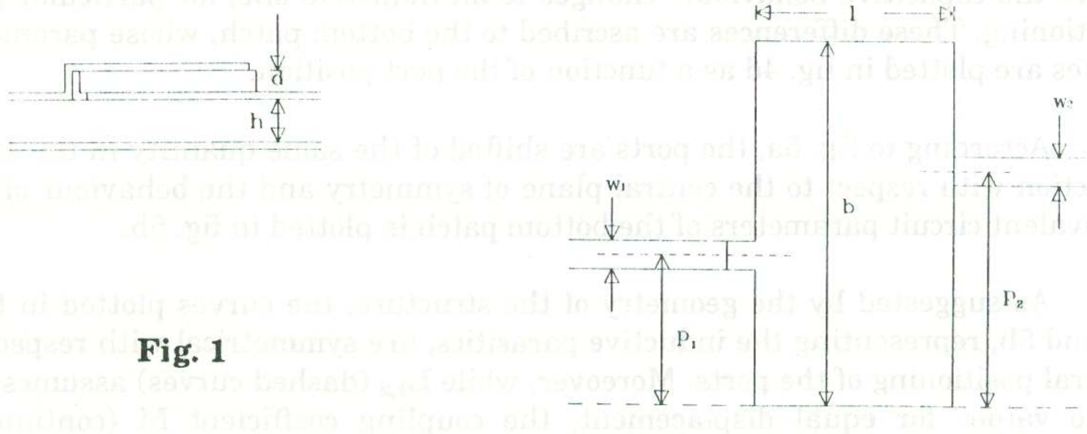

Fig. 1

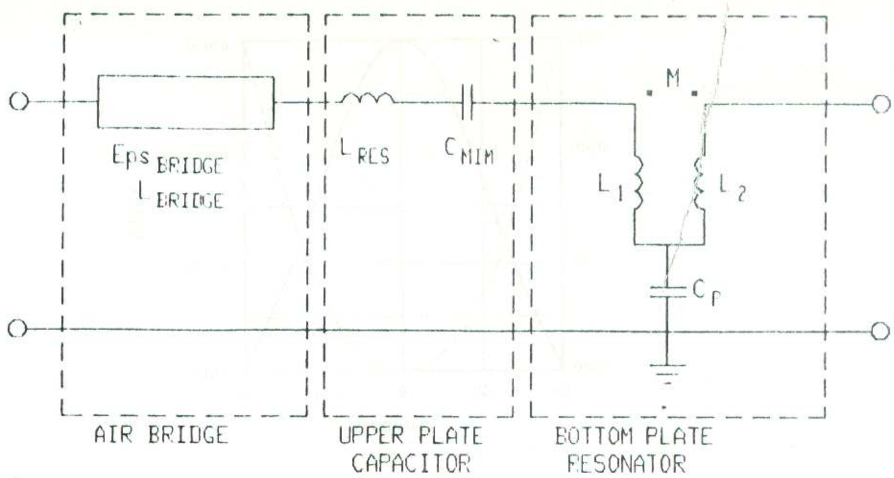

Fig. 2

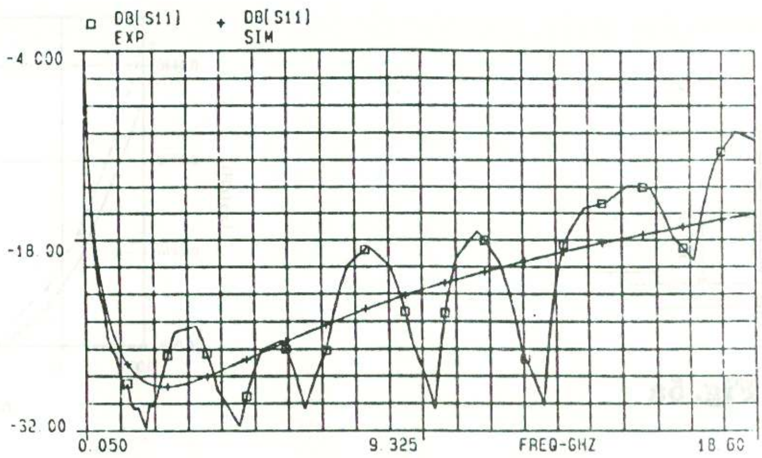

Fig. 3

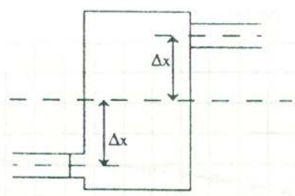

Fig. 4a

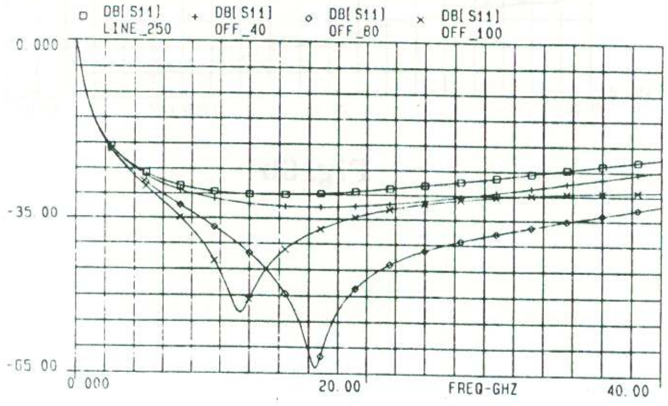

Fig. 4b

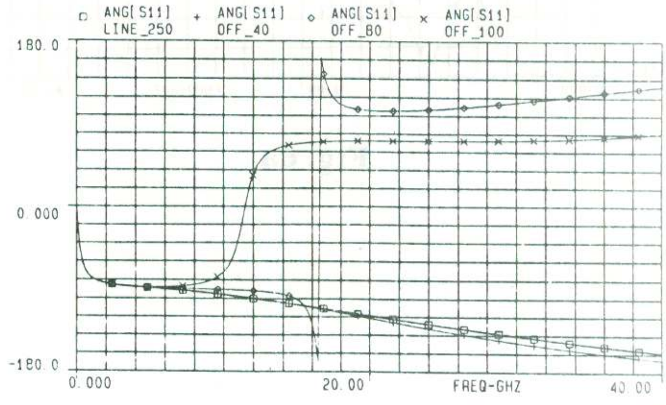

Fig. 4c

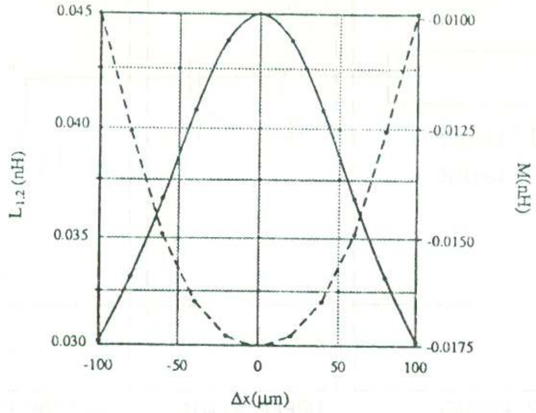

Fig. 4d

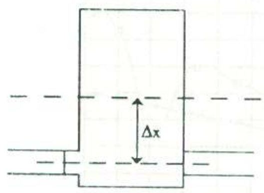

Fig. 5a

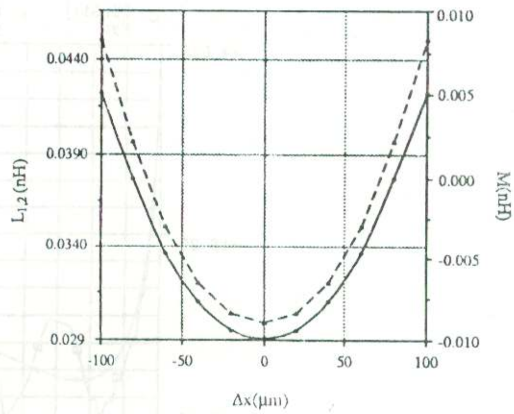

Fig. 5b

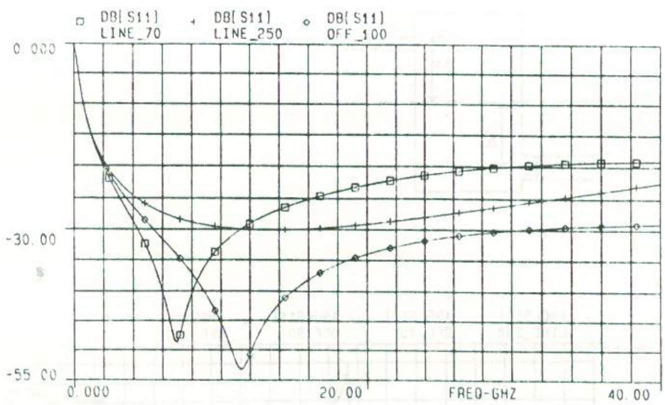

Fig. 6a

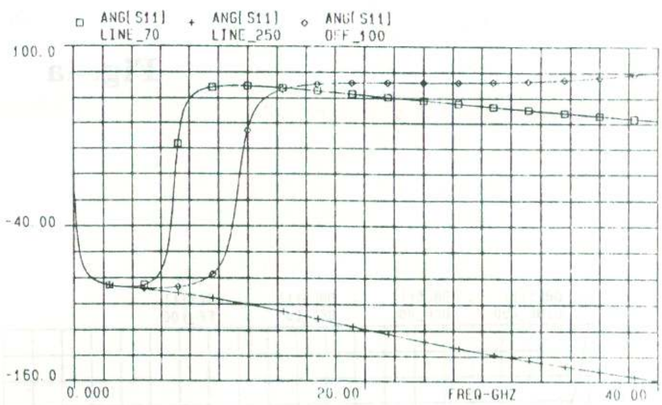

Fig. 6b